



An iron–carboxylate-based metal–organic framework for Furosemide loading and release

Yanita Devi¹, Ignatius Ang¹, Felycia Edi Soetaredjo^{1,2}, Shella Permatasari Santoso^{1,2,*} , Wenny Irawaty¹, Maria Yuliana¹, Artik Elisa Angkawijaya³, Sandy Budi Hartono¹, Phuung Lan Tran-Nguyen⁴, Suryadi Ismadji^{1,2}, and Yi-Hsu Ju^{2,3,5}

¹Department of Chemical Engineering, Widya Mandala Surabaya Catholic University, Kalijudan 37, Surabaya 60114, Indonesia

²Department of Chemical Engineering, National Taiwan University of Science and Technology, No. 43, Sec. 4, Keelung Rd., Da'an District, Taipei City, Taiwan

³Graduate Institute of Applied Science and Technology, National Taiwan University of Science and Technology, No. 43, Sec. 4, Keelung Rd., Da'an District, Taipei City, Taiwan

⁴Department of Mechanical Engineering, Can Tho University, 3-2 Street, Can Tho City, Vietnam

⁵Taiwan Building Technology Center, National Taiwan University of Science and Technology, No. 43, Sec. 4, Keelung Rd., Da'an District, Taipei City, Taiwan

Received: 24 January 2020

Accepted: 28 June 2020

Published online:

6 July 2020

© Springer Science+Business Media, LLC, part of Springer Nature 2020

ABSTRACT

An iron–carboxylate-based metal–organic framework, Fe-MIL100, has been synthesized using acid-free solvent at room temperature. Fe-MIL100 was prepared by combining Fe/H₃BTC/NaOH/H₂O (H₃BTC = trimesic acid) at a molar ratio of 1.5:1.0:*x*:880, where *x* is the varied NaOH concentration at 1.5, 3.0, and 5.0 M. The effect of NaOH molar concentration on the formation of Fe-MIL100 was studied. Characterizations of the Fe-MIL100 were carried out using powder X-ray diffraction (XRD), scanning electron microscopy (SEM), nitrogen (N₂) adsorption–desorption, and thermogravimetry analysis (TGA). The obtained Fe-MIL100, with *x* NaOH of 3.0 M, has an octahedral crystal shape (*a* = 73.41 Å), crystal size ranging from 100 to 400 nm, BET surface area of 1,446.4 m²/g, a pore volume of 0.829 cm³/g, and thermal degradation temperature of 358 °C. The potential of Fe-MIL100, a drug carrier device, was tested against Furosemide (a loop diuretic). As studied using the Langmuir adsorption isotherm model, 392.4 mg of Furosemide can be loaded per g of Fe-MIL100. The kinetic release of Furosemide was examined at 2 different biological pH of 5.8 and 7.4. The release profile of Furosemide was recorded within 24 h; it was found that the release profile follows the pseudo-first-order kinetics at pH 5.8 with a percent cumulative release of 41.56% and Korsmeyer–Peppas model at pH 7.4 with a percent cumulative release of 68.46%. The electrostatic repulsion drove the release of Furosemide from Fe-MIL100 due to the same negative

Yanita Devi and Ignatius Ang have contributed equally.

Address correspondence to E-mail: shella_p5@yahoo.com

<https://doi.org/10.1007/s10853-020-05009-3>

charge of the compounds. Fe-MIL 100 at low concentration ($< 30 \mu\text{g}/\text{mL}$) shows good biocompatibility toward the 7F2 normal cell lines.

Introduction

Metal–organic frameworks (MOFs) are porous inorganic particles, they are consisting of networks of multidentate ligands that hold the metal cluster as the central building blocks. MOFs have exciting features such as high surface area, high and adjustable porosity, and high crystallinity. Owing to those features, MOFs have excellent adsorptive and absorptive capability [1–4]. For instance, the presence of MOFs in CO_2 photoreduction systems can improve the CO_2 adsorption capacity [3]. In the water desalination membrane, the addition of MOFs helps to improve desalination performance by increasing adsorption capacity toward solutes [2]. In drug-delivery systems, the high adsorption capacity of MOFs allows high drug loading capacity [5, 6]. In this study, the utilization of MOF as a drug carrier will be pursued further. Although the use of MOF as a drug carrier has been widely developed, the opportunity is still extensive, predominantly the Material of Institute Lavoisier (MIL) family (specifically Fe-MIL100) [7].

Fe-MIL100 is an iron–carboxylate MOF which comprises Fe as the metal center and trimesic acid (benzene-1,3,5-tricarboxylic acid, abbreviated as H_3BTC) as the ligand linker. Previously, the synthesis of Fe-MIL100 involves the use of hydrofluoric acid (HF) or nitric acid (HNO_3) solvent, which is harmful and hazardous. A more sustainable approach in the synthesis of Fe-MIL100 has been proposed by Guesh and group, where sodium hydroxide (NaOH) solution was used as the solvent instead of HF or HNO_3 [8]. This sustainable approach has a synergistic effect on the biocompatibility of Fe-MIL100. The use of Fe-MIL100 as a drug carrier can give several advantages; that is, the presence of Fe transition metals is essential for many biological processes [9], and H_3BTC ligand has been found to be non-toxic and biocompatible [10], suitable for small or big molecules drug, and suitable for hydrophilic or hydrophobic drugs.

Low solubility and permeability are the main obstacles that limit the efficiency of therapeutic drugs. More than 40% of the New Chemical Entities

(NCEs) have been developed to match the evolution of diseases that require rapid treatment [11]. However, most of them inherit similar therapeutic efficiency constraints; a drug-delivery system is needed to resolve the issue. Furthermore, the proper drug-delivery system can help to deliver drugs to the designated target safely. The drug-delivery system is involving the use of a drug carrier to load and releasing the drug [12]. A considerable amount of drug carriers has been developed within the past few years (e.g., organic compounds and polymers), yet most of them possess a low loading capacity due to the limited structural adjustment and poor absorptive sites [5, 6, 13]. Fe-MIL100 has been reported to be a potential drug carrier for Aspirin, Isoniazid, Doxorubicin, Aceclofenac, and Ibuprofen [14–17]. In this work, Fe-MIL100 is applied as a drug carrier for Furosemide. Furosemide is a loop diuretic drug that uses to treat hypertension and relieves swelling caused by heart failure, liver disease, and kidney disease. Similar to other loop diuretics, Furosemide has low solubility in aqueous solution, that is only $0.18 \text{ mg}/\text{mL}$ at pH 2.3 and $13.36 \text{ mg}/\text{mL}$ at pH 10 [18]. Several techniques have been carried out to optimize the delivery of Furosemide, such as using co-solvents, pH control, nano-encapsulation, solid dispersion, complexation with cyclodextrin, microcrystalline cellulose, and composite hydrogels [19–25]. Nevertheless, most of the results are yet satisfying. Some techniques experience a burst-release effect that can decrease drug efficiency [26]. Also, there is a possibility of agglomeration with the use of micronized particles (especially in solid dispersion technique), which can result in health complications [27].

To the best of our knowledge, the drug-delivery system of Furosemide utilizing tunable particle (i.e., Fe-MIL100) has not been studied. The applicability of Fe-MIL100 as a drug carrier for Furosemide is being investigated; various mathematical models were applied for Furosemide loading and release. Fe-MIL100 was synthesized via a modified (safer) route as proposed by Guesh et al., where NaOH basic solution was used as the solvent in the synthesis instead of acid solvent [8]. It has been noted that the

presence of NaOH plays an essential role in the synthesis of Fe-MIL100; however, the influence of NaOH amount on the formation of Fe-MIL100 is still unclear. In this work, the effect of NaOH was examined on the synthesis process and the characteristics of the product.

Materials and methods

Materials

The chemicals used to prepare Fe-MIL100 were iron (II) sulfate heptahydrate ($\text{FeSO}_4 \cdot 7\text{H}_2\text{O}$, 99%), trimesic acid, or H_3BTC ($\text{C}_9\text{H}_6\text{O}_6$, 95%), and sodium hydroxide (NaOH, 97%). Ethanol ($\text{C}_2\text{H}_6\text{O}$, 99.5%) was used as the solvent, while sodium chloride (NaCl, 99%), potassium chloride (KCl, 99%), sodium phosphate dibasic dihydrate ($\text{Na}_2\text{HPO}_4 \cdot 2\text{H}_2\text{O}$, 99.5%), sodium phosphate monobasic monohydrate ($\text{NaH}_2\text{PO}_4 \cdot \text{H}_2\text{O}$, 99%), and potassium phosphate monobasic (KH_2PO_4 , 99%) were used to prepare the buffer solutions. Furosemide ($\text{C}_{12}\text{H}_{11}\text{ClN}_2\text{O}_5\text{S}$, 98%) was chosen as the drug model for loading and release study. All the chemicals used in this study were purchased from Sigma-Aldrich and were directly used without further purification.

Synthesis of Fe-MIL100

The synthesis method by Guesh et al. was adopted for preparing Fe-MIL100 with slight modification [8]. H_3BTC (7.6 mmol) was dissolved using NaOH solution at three different molar concentrations (1.5, 3.0, and 5.0 M). Meanwhile, $\text{FeSO}_4 \cdot 7\text{H}_2\text{O}$ (11.4 mmol) was dissolved in deionized water; then, it was added dropwise to the previously prepared H_3BTC solution. The final mixture has a molar ratio of $\text{Fe}/\text{H}_3\text{BTC}/\text{NaOH}/\text{H}_2\text{O}$ of 1.5:1: x :880, where $x = 1.5, 2.5, 3.0, 4.0,$ and 5.0. The synthesis was carried out at room temperature (30 °C) under constant stirring conditions (200 rpm) for 24 h. The resulting solids were separated from the solution using Thermo Scientific Medifuge centrifuge at 3,700 rpm for 15 min. Subsequently, the solids were washed using reverse osmosis water and ethanol for 3–5 times and then soaked in water for 1 h under constant stirring at 60 °C. The resulting products were collected and placed in a vacuum oven at 80 °C for 6 h.

Characterization of Fe-MIL100

The crystallinity pattern of the samples was recorded using Philips X'pert X-ray Diffractometer with a copper $\text{K}\alpha$ radiation source ($\lambda = 1.5425 \text{ \AA}$) at 40 kV and 30 mA. Subsequently, Rietveld refinement analysis was conducted on the obtained XRD pattern of samples using a computer program Match! (version 3.8.3.151 64-bit) [28]. The surface morphology images were acquired by a JEOL JSM-6500F Field Emission Scanning Electron Microscopy. The BET surface area and total pore volume were measured by N_2 adsorption–desorption using Quantachrome's Quadrasorb SI at $-196 \text{ }^\circ\text{C}$, and the outgassing process was conducted at 200 °C for 6 h. Thermal stability was analyzed using thermal gravimetric analysis (TGA) in a PerkinElmer TGA 8000, at the temperature range of 26.7–600 °C with a heating rate of 10 °C/min under nitrogen gas flow (20 mL/min).

Adsorption kinetic experiments

Fe-MIL100 was dried overnight at 110 °C prior to the experiment. 70 mg of Furosemide was dissolved in 100 mL ethanol. 20 mg of dried Fe-MIL100 was introduced to the prepared Furosemide solution. The adsorption was conducted for 12 h at room temperature in a shaking water bath (Memmert SV-1422). An aliquot of the solution was taken within a specific time interval to measure the residual Furosemide concentration. The residual concentration of Furosemide was measured using a direct UV–Vis spectrophotometer measurement at a wavelength of 286 nm, without the addition of reagents.

The amount of Furosemide adsorbed at a specific time (q_t) was calculated using Eq. (1) as follows:

$$q_t = \frac{(C_0 - C_t)V}{W} \quad (1)$$

where C_0 is the initial concentration of Furosemide, and C_t is the residual concentration of Furosemide at a specific time (mg/L). V is the total volume of solution (L), and w is the amount of Fe-MIL100 (g).

Adsorption isotherm experiments

The adsorption isotherm experiments were carried at various initial concentrations of Furosemide (25 to 300 mg/L). 20 mg of Fe-MIL100 was introduced into 100 mL of prepared Furosemide solution. Adsorption was conducted for 12 h at room temperature in a

water bath shaker. The residual concentration of Furosemide was measured using a UV–Vis spectrophotometer at a wavelength of 286 nm. The equilibrium amount of Furosemide adsorbed (q_e) was calculated using Eq. (2) as follows:

$$q_e = \frac{(C_0 - C_e)V}{W} \quad (2)$$

where C_e is concentrations of Furosemide at equilibrium (mg/L).

Loading and release experiments

The loading experiments were carried out by adding a certain amount of Fe-MIL100 into the Furosemide solution under stirring for 12 h. Furosemide-loaded Fe-MIL100 was separated from the solution by centrifugation at 3700 rpm for 15 min. The solid was washed using reverse osmosis water and ethanol, and then placed in a vacuum oven at 80 °C until dry for 6 h. Release experiments were carried out using the dialysis membrane under the stirring condition at 37 °C for 12 h in two different phosphate buffer pH of 5.8 (to simulate large intestine fluid) and 7.4 (to simulate small intestine fluid).

An aliquot (3 mL) of the solution was taken within a specific time interval to measure the Furosemide concentration released. Subsequently, 3 mL of fresh buffer solution was added to maintain the same volume of the system. The sample was diluted several times before analyzed using Shimadzu UV mini-1240 Spectrophotometer at 286 nm.

The release of Furosemide from the adsorbent was calculated using Eq. (3) as follows:

$$\% \text{Release} = \frac{C_t}{C_0} \times 100\% \quad (3)$$

where C_t and C_0 are the released and initial concentrations of Furosemide loaded in Fe-MIL100 (mg/L), respectively.

Biocompatibility assay

The biocompatibility of the synthesized Fe-MIL 100 was tested against mouse bone marrow cells 7F2. Different doses of Fe-MIL 100 were introduced to cell culture, which is 10, 25, 30, 50, 75, 100, and 125 µg/mL. Cell viability was determined 12, 24, and 48 h after incubation in media containing Fe-MIL 100. The detailed culture procedures can be found elsewhere [29]. After incubation, 20 µL of 5 mg/mL MTT in PBS

was added to the culture and then incubated for 4 h. The MTT mixed media were then replaced with 0.2 mL DMSO. Cell viability (%) is then calculated as Eq. (4):

$$\% \text{Cell viability} = \frac{\text{Abs}_i}{\text{Abs}_0} \times 100\% \quad (4)$$

where Abs_i is the absorbance of the cell, and Abs_0 is the absorbance of the blank. The absorbance was measured at 570 nm using a microplate reader Biotek PowerWave XS.

Results and discussion

Effect of NaOH in the formation of Fe-MIL100

Conventionally, Fe-MIL100 is synthesized using hazardous solvents (i.e., HF or HNO₃) via a solvothermal process which requires high thermal energy. A sustainable synthesis route for Fe-MIL100 using an amiable solvent (NaOH solution) and low (room) temperature overcomes the conventional synthesis method. In the formation of Fe-MIL100, H₃BTC acts as a Fe binding ligand. Prior to the binding, deprotonation of H₃BTC must occur; this results in the formation of BTC (deprotonated H₃BTC) species, which are negatively charged ligands that lose 3 H⁺ ions. The difference in charge between BTC (negative charge) and Fe (positive charge) encourages the formation of the metal–organic networks. In conventional synthesis, high thermal energy is needed to deprotonate both the ligand and acid (as the complexation modulator). Meanwhile, in the use of NaOH solvent, the basicity of NaOH facilitates the ligand deprotonation without the need of high thermal energy [30]. NaOH played an essential modulatory role in the synthesis of Fe-MIL100 under the basic condition and low temperature. A suitable amount of NaOH results in the favorable formation of Fe-MIL100; partial deprotonation might occur if the amount of NaOH is too small, and the formation of metal hydroxide species can arise if the amount of NaOH is excessive [31–33]. Thus, it is crucial to evaluate the effect of the amount of NaOH on the formation of Fe-MIL100.

NaOH acts as a deprotonating agent for H₃BTC by substituting the H⁺ ions with Na⁺ ions, thus forming Na₃BTC. The deprotonation of H₃BTC occurs when

the pH of the solution exceeds the acid dissociation constant (pKa) [4], where The pKa values of the H_3BTC in a sequence are 3.12, 3.89, and 4.70. Furthermore, the deprotonation of H_3BTC can increase the solubility of the compound. As NaOH was added dropwise, the insoluble H_3BTC solution (with white solid particles observed) starts to dissolve, and eventually, crystal clear solution was obtained (Fig. 1a). Next, Fe solution was added to the dissolved ligand solution. A decrease in final solution pH was observed after metal addition (Fig. 1b); this is since metal is a Lewis acid. The highest Fe-MIL100 yield is obtained from the mixture with a final pH of 5.8, which is the Fe-MIL100 synthesized with NaOH at $x = 3.0$.

The amount of NaOH added is affected by the yield of Fe-MIL100 (Fig. 1b). Fe-MIL100, which synthesized with NaOH at $x = 1.5$, gives the lowest yield (36.60%). The %yield obtained from the other variation, $x = 3.0$ and 5.0, were 66.00% and 55.61%, respectively. The low yield of Fe-MIL100 at $x = 1.5$ is because there is not enough NaOH to deprotonate and dissolve the linker fully; this was visually indicated by the appearance of white solids (insoluble organic ligand) shortly after the metal solution is

added. The unreacted ligand was then washed using water/ethanol to remove it. A similar phenomenon was observed during Fe-MIL100 synthesis using NaOH at $x = 2.5$. Full linker deprotonation (complete dissolution) was obtained using NaOH at $x = 3.0$, and 5.0. Even though NaOH at $x = 5.0$ was capable of dissolving the mixture completely, it was found that the presence of excess NaOH may promote the formation $Fe(OH)_3$ as a by-product [34].

The %yield (Fig. 1b) shows that NaOH at $x = 1.5$ gives the lowest yield, followed by $x = 5.0$. NaOH at $x = 2.5$ and 4.0 gives an intermediate yield, while at $x = 3.0$ is the highest. In the subsequent characterization study, MIL-100 (Fe) produced using $x = 1.5$, 3.0, and 5.0 will be further evaluated because the three samples provide the most remarkable yield differences, whereas MIL-100 (Fe) with NaOH at $x = 2.5$ and 4.0 are not used.

Characterization of MIL-100(Fe)

Powder XRD patterns of the synthesized Fe-MIL100 samples were observed to evaluate the influence of NaOH. As shown from the XRD results in Fig. 2, Fe-MIL100 synthesized at a different molar ratio of

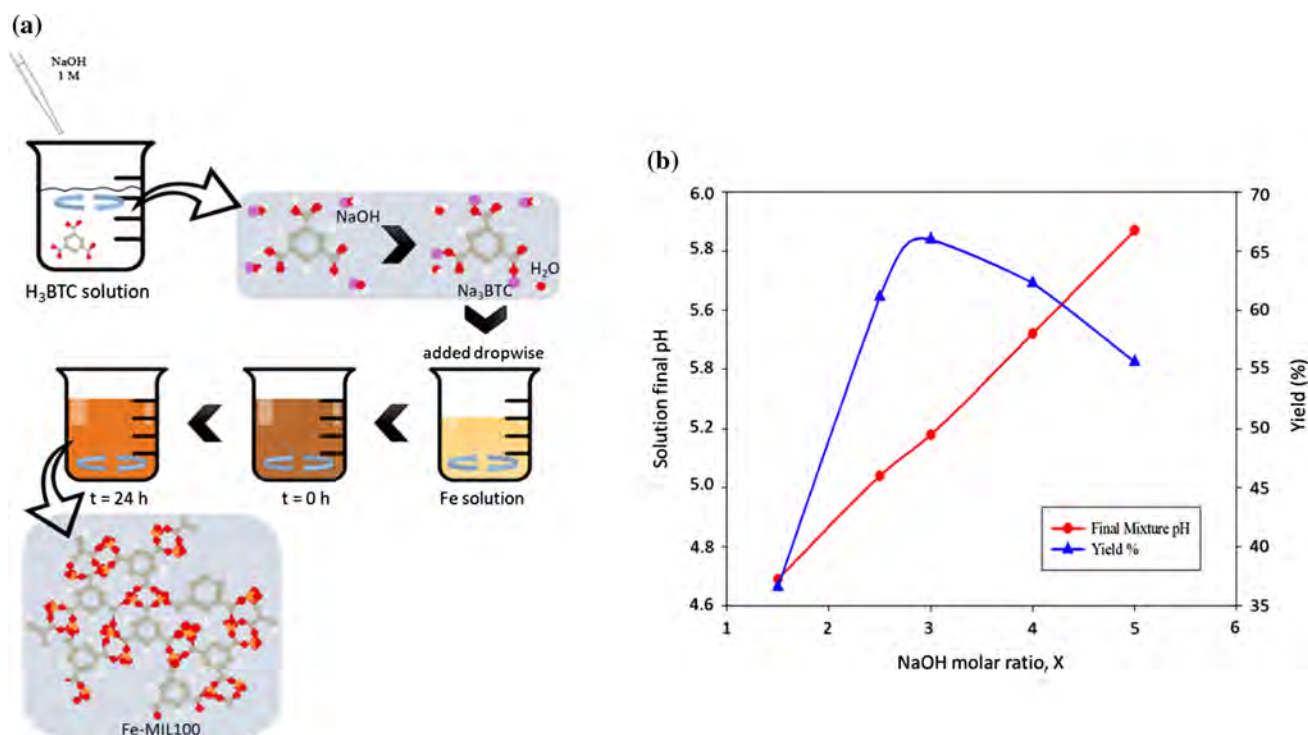


Figure 1 a Schematic diagram illustrating the physical appearance change of Fe and H_3BTC mixture due to the addition of NaOH, in the synthesis of MIL-100(Fe). b The curve showing the effect of NaOH molar ratio on the formation of Fe-MIL100.

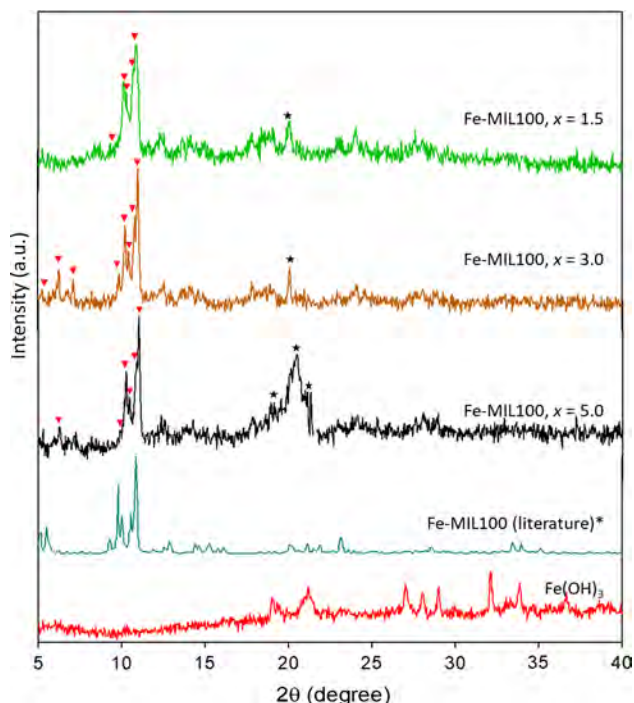


Figure 2 XRD patterns of the synthesized Fe-MIL100 at various molar ratios of NaOH, reported Fe-MIL100, and Fe(OH)₃. The asterisks ▼ indicate the peaks that belong to the Fe-MIL100; asterisks ★ indicate the peaks that belong to the iron hydroxide. * The XRD of Fe-MIL 100 based on published literature [36].

NaOH ($x = 1.5, 3.0,$ and 5.0) exhibits quite similar patterns. A Rietveld refinement was conducted to match the XRD pattern of the samples against Fe-MIL100 from the database, and the matching results were given in Supplementary Data Figure S1–S3. The goodness of fit of the Rietveld refinement is presented in Table S1. It is noted that Fe-MIL100 $x = 1.5$ and $x = 3.0$ have lower Bragg R-factor and Chi-square (χ^2), and this indicates that the observed and calculated patterns can converge well. However, Fe-MIL100, with $x = 3.0$, shows a better correlation, which is indicated by the higher peak matching with the selected phase from the database (Table S1). The synthesized Fe-MIL100, with $x = 3.0$, has a better pattern match to the reference database. Fe-MIL100, $x = 5.0$, exhibits different patterns from the reported one, precisely the appearance of peaks detected in the 2θ range of 19.95 to 21.23 degrees. The synthesized Fe-MIL100, $x = 3.0$, has the highest product yield and shows remarkable peak similarities to the XRD pattern of the literature. Furthermore, the calculated unit cell (a) for the Fe-MIL100, $x = 3.0$, is 73.41 Å which is in a good accordance with the a of the reference

($a = 73.34$ Å) [35, 36]. The difference in the XRD profile between conventional and synthesized (in this study) Fe-MIL 100 could be due to differences in the solvent used. NaOH solution used in the synthesis of Fe-MIL 100 initiates the formation of metal hydroxide, which affects the XRD pattern, whereas the formation of metal hydroxide does not occur in the conventional Fe-MIL 100 which prepared using HF solvent [8].

The as-synthesized Fe-MIL100, $x = 3.0$, has octahedral shaped particles with a crystal size ranging from 100 to 400 nm (Fig. 3b), which is similar to the reported literature [8, 15, 36, 37]. The non-homogeneous crystal size and shape of the obtained Fe-MIL100 are acceptable, considering that the synthesis process was conducted at room temperature (not thermostatted) and without strict control of sudden stirring acceleration. In the case of high homogeneity, Fe-MIL100 particles are desirable, and the synthesis must be conducted at an elevated temperature where better nucleation and crystal growth occur [38]. Fe-MIL 100, $x = 1.5$, shows smaller particle sizes and more irregular shapes (Fig. 3a), which could be due to structural collapse. Similarly, for Fe-MIL 100, $x = 5.0$, irregular particle shapes were also observed (Fig. 3c), which could be related to the presence of metal hydroxide particles.

Based on the N₂ adsorption–desorption isotherm (Fig. 4), the synthesized Fe-MIL100 shows a step increase at low relative pressure ($P/P_0 < 0.2$), which demonstrates the presence of micropore structures [39]. Brunauer–Emmett–Teller (BET) surface area and total pore volume of Fe-MIL100 were determined from the N₂ isotherm data by utilizing the following Eqs. (5) and (6):

$$\frac{1}{[V_a(\frac{P}{P_0} - 1)]} = \frac{C - 1}{V_M C} \times \frac{P}{P_0} + \frac{1}{V_M C} \quad (5)$$

where P is the partial vapor pressure of adsorbate gas in equilibrium (Pa), P_0 is the saturated vapor pressure of adsorbate gas (Pa), C is the dimensionless constant, V_a is the volume of gas adsorbed onto the adsorbent at STP (cm³/g), and V_M is the volume of gas adsorbed into the adsorbent to form a monolayer at STP (cm³/g).

$$S_{\text{BET}} = \frac{V_M N_a A_m}{V_m} \quad (6)$$

where S_{BET} is the BET surface area (m²/g), N_a is the Avogadro's number, A_m is the cross-sectional area of

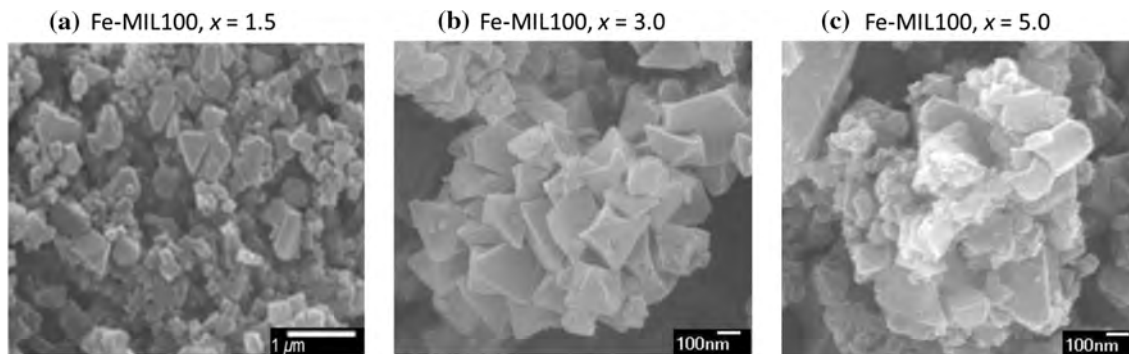


Figure 3 SEM image of synthesized Fe-MIL100 at various molar ratios of NaOH.

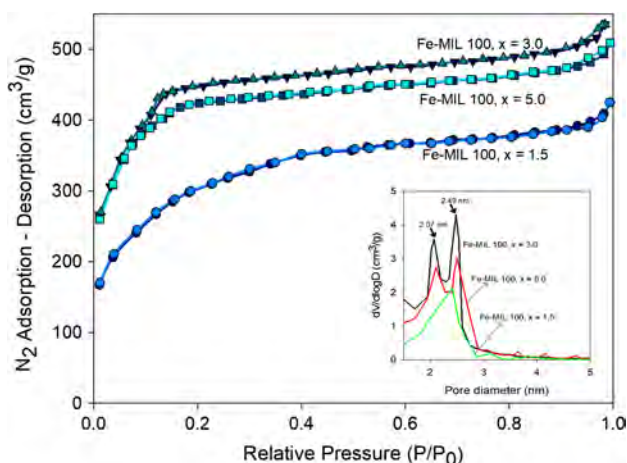


Figure 4 N₂ adsorption–desorption isotherm of Fe-MIL100 with NaOH at $x = 3.0$. The inset figure shows the pore size distribution of Fe-MIL 100.

the adsorbate (m^2), and V_m is the molar volume (cm^3). The calculation of the total pore volume (TPV) was carried out using Eq. (7) as follows:

$$TPV = \frac{V_{sat} \rho_{vap}}{\rho_{liq}} \quad (7)$$

where V_{sat} is the volume of N₂ adsorbed into the adsorbent at saturation (cm^3/g), ρ_{vap} is the density of N₂ at STP ($g L^{-1}$), and ρ_{liq} is the density of liquid N₂ at boiling point (g/L). BET surface area and total pore volume of Fe-MIL100, $x = 3.0$, are found to be 1446.4 m^2/g and 0.829 cm^3/g , respectively. The BET surface area of Fe-MIL100 at $x = 1.5$ and 5.0 is found to be 1354.6 and 1052.9 m^2/g , respectively; the total pore volume of the corresponding materials is 0.827 and 0.831 cm^3/g . Meanwhile, the reported Fe-MIL100 exhibits a BET surface area and total pore volume of 1604.8 m^2/g and 0.67 cm^3/g , respectively [29, 39]. The obtained BET parameters are quite different from

that of reported literature (Fe-MIL100 produced using the conventional method), which may be due to the differences in the synthesis method and solvent used [8, 15, 36, 37]. The pore size distribution curve (inset Fig. 4) of the synthesized Fe-MIL100 ($x = 3.0$) shows two peaks centered at 2.07 and 2.49 nm, indicating the occurrence of mesoporous cages which is the main characteristic of Fe-MIL100. The mesoporous cages were also observed for Fe-MIL100 synthesized with NaOH at $x = 5.0$, but not for Fe-MIL100 with NaOH at $x = 1.5$. Considering that Fe-MIL100, $x = 3.0$, has the highest product yield and good similarity in characteristics (based on XRD and N₂ sorption) with reference material, this sample is further investigated.

TGA curve (Fig. 5) shows that Fe-MIL100, $x = 3.0$, has excellent thermal stability, where thermal degradation is starting to occur after 358 °C (15.9% weight loss). Three stages of thermal degradation were observed for Fe-MIL100, $x = 3.0$, which is at

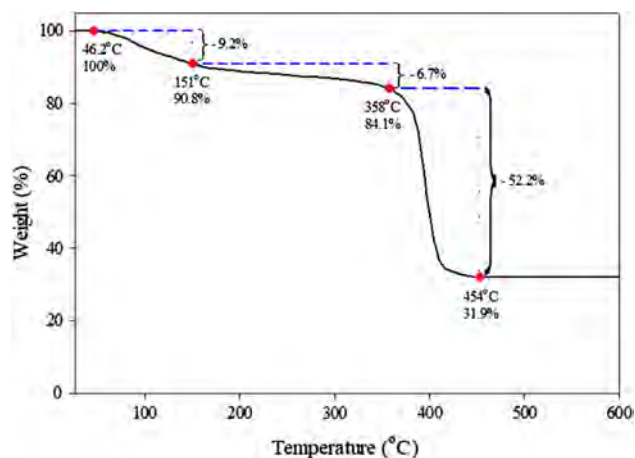


Figure 5 Thermal gravimetric analysis (TGA) curve of synthesized Fe-MIL100, $x = 3.0$.

46.2–151 °C, 151–358 °C, and 358–454 °C. The first stage, with a weight loss of 9.2%, is attributed to the evaporation of water and volatile guest molecules (i.e., ethanol). The second stage, a weight loss of 6.7%, is attributed to the dehydration of water coordinated with the iron trimers. Finally, significant weight loss (52.2% by weight) in the range of 358–454 °C is related to the decomposition of the organic linker in Fe-MIL100. The decomposition of this stage also marks the breakdown of coordination between metals and the linker, which then causes structural collapse and leaves metal oxide as the final residue.

Adsorption kinetic

Comprehensive details about the adsorption of Furosemide on Fe-MIL100 can be evaluated through the adsorption kinetic results. The pseudo-first- and pseudo-second-order models were used to correlate the kinetic data. The nonlinear form of pseudo-first- and pseudo-second-order is shown in Eqs. (8) and (9), respectively:

$$q_t = q_e(1 - e^{-k_1 t}) \quad (8)$$

where t is the adsorption time (h), and k_1 is the pseudo-first-order rate constant (h^{-1}).

$$qt = \frac{q_e^2 k_2 t}{1 + q_e k_2 t} \quad (9)$$

where k_2 is the pseudo-second-order rate constant (g/mg h). A fitting using nonlinear regression was used to determine the pseudo-first- and pseudo-second-order parameters [40].

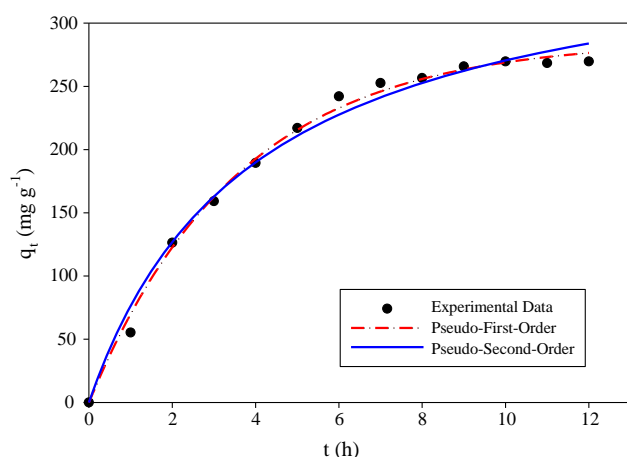


Figure 6 Adsorption kinetics of Furosemide using Fe-MIL100, $x = 3.0$, plotted to pseudo-first- and pseudo-second-order.

The nonlinear plot in Fig. 6 shows that the adsorption of Furosemide using Fe-MIL100 occurs rapidly at the first 6 h adsorption time and gradually slower over time. The rapid adsorption during the beginning is due to the high availability of vacant sites of adsorbent [41, 42]. Meanwhile, as adsorption proceeded, the availability of vacant sites decreases as more Furosemides are adsorbed, which further leads to an equilibrium state [42]. The sum squared error (R^2) in Table 1 shows that pseudo-first-order is favorably over pseudo-second-order to represent the kinetic adsorption of Furosemide on Fe-MIL100. Furthermore, the experimented q_e value is also closer to the fitting q_e value of pseudo-first-order than pseudo-second-order. Better fitting to pseudo-second-order suggests that chemisorption is the rate-controlling step in this process.

Adsorption isotherm

The adsorption isotherm is studied to understand the adsorption phenomenon and mechanism. Langmuir and Freundlich isotherm models are used to represent Furosemide adsorption isotherm on Fe-MIL100. The Langmuir equation applies to the adsorption on completely uniform surfaces, regardless of the interaction between adsorbed molecules. The Langmuir equation model is expressed as follows:

$$q_e = \frac{q_{\max} k_L C_e}{1 + k_L C_e} \quad (10)$$

where q_{\max} is the theoretical maximum amount of Furosemide adsorbed into the adsorbent (mg/g) often called as the adsorption capacity of the adsorbent, k_L is the Langmuir constant (L/mg), and C_e is the concentration of the remaining Furosemide in solution at equilibrium (mg/L) [43]. The Freundlich adsorption isotherm is an equation model for heterogeneous adsorbent, and the equation is expressed as follows:

$$q_e = k_F C_e^{1/n} \quad (11)$$

where k_F is the Freundlich constant (mg/g) (L/mg) $^{1/n}$, and n is related to the adsorption intensity [43].

The experimental data fitting to both isotherm models is given in Fig. 7, and all the parameters from the model are summarized in Table 2. Based on R^2 value, it was obtained that the Langmuir model is more suitable for describing the adsorption of Furosemide on Fe-MIL100. This indicates that

Table 1 Calculated adsorption kinetic parameters of Furosemide on Fe-MIL100, $x = 3.0$

Initial concentration (mg L ⁻¹)	$q_{e, \text{exp}}$ (mg g ⁻¹)	Pseudo-first-order			Pseudo-second-order		
		$q_{e1, \text{cal}}$ (mg g ⁻¹)	k_1 (h ⁻¹)	R^2	$q_{e2, \text{cal}}$ (mg g ⁻¹)	k_2 (g mg ⁻¹ h ⁻¹)	R^2
70	269.7	286.6	0.279	0.995	377.3	0.001	0.988

Adsorption condition: $T = 30$ °C, $C_0 = 20$ mg

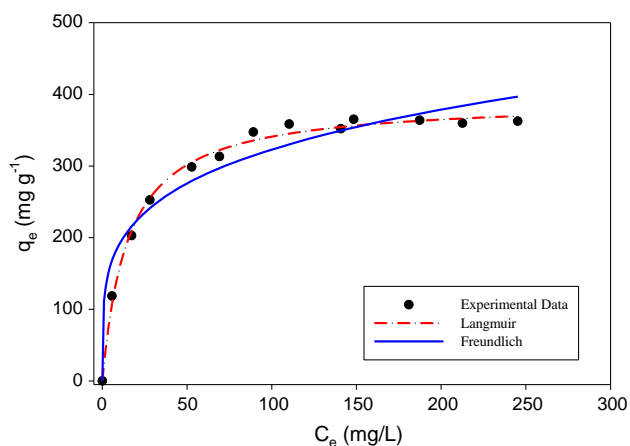


Figure 7 Adsorption isotherm of Furosemide using Fe-MIL100, $x = 3.0$, plotted to Langmuir and Freundlich equations.

Furosemide adsorbed by forming a monolayer on homogeneous adsorption sites of Fe-MIL100. The Langmuir constant shows a relatively low value ($k_L = 0.067$ L/mg), which indicates that the affinity between Fe-MIL100 as adsorbent and Furosemide is small [41].

Loading and release of Furosemide

Furosemide was loaded on Fe-MIL100 using ethanol as a solvent; this is since Furosemide is highly soluble in ethanol compared to other solvents. For instance, the solubility of Furosemide in the water at 30 °C is 25.32 mg/L, while its solubility in ethanol is $> 2.25 \times 10^3$ mg/L [44]. Generally, drugs with low solubility in aqueous solutions tend to have a high affinity with the hydrophobic pores of the MIL family

[7]. Based on batch adsorption experiments, the amount of Furosemide loaded on Fe-MIL100 is 0.2697 mg of Furosemide per mg of Fe-MIL100, and the loading efficiency is 67.55%.

In vitro release of Furosemide was studied in two different pHs of phosphate buffer solutions, that are 5.8 and 7.4, respectively. The release of Furosemide (at the stated pHs) is driven by the electrostatic repulsion between negative charged Furosemide and Fe-MIL100. Furosemide is a weak acid with a pKa value of 3.8; thus, the release of Furosemide at a pH of 5.8 and 7.4 will cause deprotonation of the carboxyl cluster since pH solution $>$ pKa [45]. Similarly, at pH 5.8 and 7.4, Fe-MIL100 exhibits negative surface charges due to partial deprotonation of carboxyl cluster in carboxylic acid of the outer surface of the particle [37, 46].

According to the release profile, as shown in Fig. 8a, there are two stages of Furosemide release from Fe-MIL100. For the profile release at pH 5.8—the first stage is a rapid release, up to 35.31% cumulative release, observed within the initial 8 h which is attributed to the release of drug located in the pore near to the outer surface of particle, and an adequate solubility of the drug in pH 5.8 (≥ 270 mg/L at 37 °C) [18]. The second stage is a slow release, up to 41.56% cumulative release, observed within the next 16 h, which indicate the release of drug located within the pores. The slower release is due to the fact that there are only a few Furosemide molecules available so that the repulsion forces weaken. For the profile release at pH 7.4—as shown in Fig. 8b, there is a distinct release profile at pH 7.4 compared to pH

Table 2 Calculated adsorption isotherm parameters of Furosemide on MIL-100(Fe), $x = 3.0$

Langmuir isotherm			Freundlich isotherm		
q_{max} (mg g ⁻¹)	k_L (L mg ⁻¹)	R^2	k_F (mg g ⁻¹) (L mg ⁻¹) ^{1/n}	n	R^2
392.4	0.067	0.995	112.5	4.364	0.954

Adsorption condition: $T = 30$ °C, $C_0 = 20$ mg

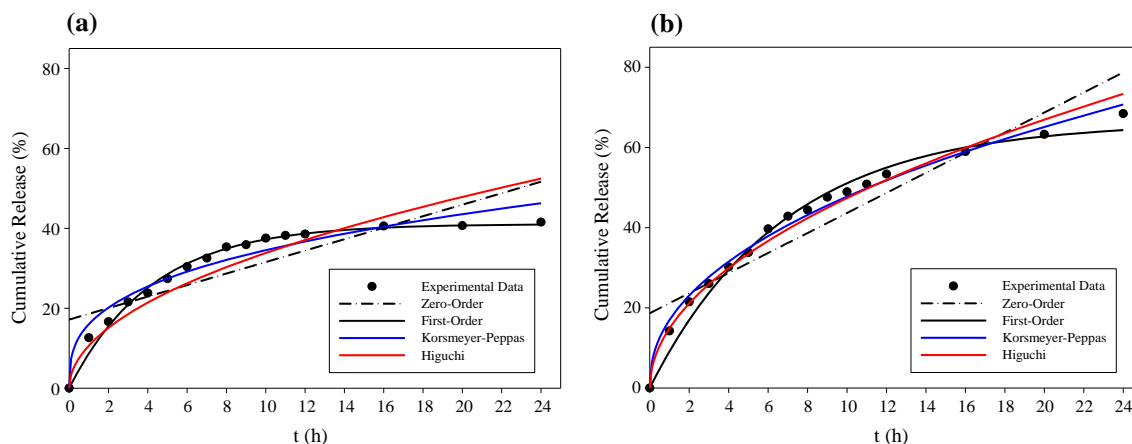


Figure 8 Release kinetic models of Furosemide from Fe-MIL100, $x = 3.0$, at **a** pH 5.8 **b** pH 7.4.

5.8. At pH 7.4, and the release of Furosemide from Fe-MIL100 keeps rising during 24 h observation, with a cumulative release of 68.46%. This is due to the high solubility of the drug in more alkaline pH ($\geq 1.9 \times 10^3$ mg/L, at 37 °C), and higher repulsion forces between the more negative charged Furosemide and Fe-MIL100 [18].

With a loading efficiency of 67.55%, the cumulative release of Furosemide using Fe-MIL100 was found to be 41.56% (at pH 5.8) and 68.46% (at pH 7.4). These results indicate that Fe-MIL100 has good potential in increasing the bioavailability of Furosemide. In a previous study, by using a matrix tablet made from polypropylene powder, the release of Furosemide only reached 37.9% (with initial loading efficiency of 73.8%) [47]. The cumulative release efficiency of Furosemide obtained in this study is also comparable to the cumulative release of other drugs loaded in Fe-MIL100. For instance, the cumulative release of Iso-niazid loaded on Fe-MIL100 after 24 h is 50.4% (at pH 5.8) and 72.2% (at pH 7.4) [15]. Cumulative release of Doxorubicin on polypyrrole-modified Fe-MIL100 is 42.7% (at pH 7.4) and 82.7 (at pH 5.0) [17].

Several kinetic models were applied to achieve particular elucidation regarding the release behaviors of Furosemide from Fe-MIL100. The models used are zero-order kinetic, first-order kinetic, Korsmeyer–Peppas, and Higuchi. The mathematical forms of the kinetic models are as follows:

$$R = R_e + k_0t \tag{12}$$

where R and R_e are the cumulative release percentage of Furosemide at specific and equilibrium time (%),

respectively. k_0 is the zero-order release constant (h^{-1}).

$$R = R_e [1 - e^{-k_1t}] \tag{13}$$

where k_1 is the first-order release constant (h^{-1}) [48].

$$\frac{M_t}{M_\infty} = k_M t^n \tag{14}$$

where $\frac{M_t}{M_\infty}$ equals to the amount of Furosemide released at specific and equilibrium time (%), respectively. k_M is the dimensionless Korsmeyer–Peppas constant, and n is attributed to the drug release mechanism [49].

$$\frac{M_t}{M_\infty} = k_H t^{1/2} \tag{15}$$

where k_H is the dimensionless Higuchi constant [29].

The calculated parameters obtained from fitting of the experimental data are given in Table 3. The release of Furosemide from Fe-MIL100 in PBS, at pH 5.8, fits the first-order kinetic model better than other models, with a high correlation coefficient value of 0.989. This indicates that the drug dissolution rate is affected by the amount of drug loaded into the particle [50]. Meanwhile, the release in PBS at pH 7.4 fits the Korsmeyer–Peppas model, with a correlation coefficient value of 0.991. The n value of 0.45 shows that the release of Furosemide from Fe-MIL100 follows the Fickian diffusion with a cylindrical geometry [51].

The stability of Fe-MIL100 was observed through the loss of Fe content in the matrix. The tests were conducted by soaking a known amount of Fe-MIL100 into PBS solution at pH 5.8 and 7.4, for 24 h; the Fe

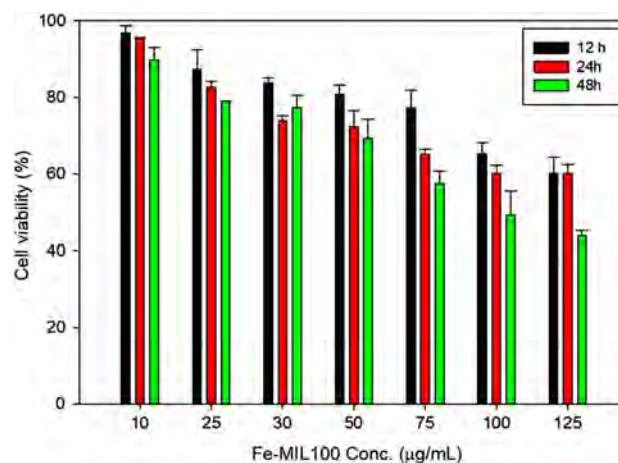
Table 3 Calculated release kinetic parameters of Furosemide from Fe-MIL100, $x = 3.0$

Release model	Parameter	Release pH	
		5.8	7.4
Zero-order	k_0 (h^{-1})	1.440	2.505
	R_e (%)	17.17	18.66
	R^2	0.675	0.849
First-order	k_1 (h^{-1})	0.237	0.148
	R_e (%)	41.10	66.27
	R^2	0.989	0.983
Korsmeyer–Peppas	k_M (h^{-n})	16.02	16.94
	n	0.334	0.450
	R^2	0.953	0.991
	R^2	0.856	0.985
Higuchi	k_H ($\text{h}^{-0.5}$)	10.71	14.98
	R^2	0.856	0.985

content was measured using ICP-AES. At pH 5.8, 1.91% of Fe is lost, while at pH 7.4, 4.37% of Fe is lost. This indicates the degradation of the matrix that occurs when Fe-MIL100 is in PBS; thus, the rapid release of Furosemide from Fe-MIL100 can be attributed to the partial matrix degradation of Fe-MIL100 in phosphate-containing solution. As studied by Bellido et al. (2014), the presence of phosphate ion from a PBS solution causes structural degradation of MIL-100(Fe) [46]. This is since phosphate ion of PBS is able to form coordination bonds with the Lewis metal centers, which cause the detach of metal from the carboxylate linker of H_3BTC [35, 52]. The more significant loss at pH 7.4 is due to more phosphate ions from PBS to form a coordination bond with the Lewis metal centers, which further leads to the gradual replacement of the carboxylate linker [35, 52].

Biocompatibility assay

The in vitro biocompatibility assay of synthesized Fe-MIL 100 (NaOH at $x = 3.0$) was evaluated against the 7F2 cell line, and the result is presented as cell viability (Fig. 9). Fe-MIL 100 with a low dose of 10 $\mu\text{g}/\text{mL}$ shows good biocompatibility toward the cell even after 24 h incubation, with cell viability 95.4%. However, prolonged incubation time causes the cell viability reduced to 89.8%. Good biocompatibility, with cell viability $> 80\%$, can be maintained up to 30 $\mu\text{g}/\text{mL}$ Fe-MIL 100 dose and 12 h incubation time. Fe-MIL 100 at higher doses and prolonged incubation

**Figure 9** Cell viability assay of Fe-MIL 100 (NaOH at $x = 3.0$) against mouse bone marrow cells 7F2, at the different dosage and incubation time.

times is potentially toxic to cells, which is indicated by cell viability below 80%. The cytotoxicity of Fe-MIL 100 can be caused by the presence of metal, which triggers the formation of reactive oxygen species that cause damage to cells [15].

Conclusion

The alkali-modified Fe-MIL100 was synthesized at room temperature (30 °C) using NaOH solution as the solvent, instead of the hazardous HF and HNO_3 . The highest yield of Fe-MIL100 of 66.00% was able to achieve from synthesis using NaOH at a molar ratio $x = 3.0$. The coordination of metal-linker, in the formation of Fe-MIL100, was driven by the deprotonation of the H_3BTC linker in the presence of ions from NaOH. The as-synthesized Fe-MIL100 exhibits a length of the unit cell edge and BET surface area of 73.41 Å and 1,446.4 m^2/g , respectively. Fe-MIL100 can be an excellent material for Furosemide adsorption, which represented well by the pseudo-first-order model (kinetically) and Langmuir model (isothermally). An amount of 0.2697 mg of Furosemide can be loaded per mg of Fe-MIL100, with a loading efficiency of 67.55%. The release profile of Furosemide from Fe-MIL100 was studied in PBS solution at two different biological pH of 5.8 and 7.4. The release of Furosemide from Fe-MIL100 in PBS at pH 5.8 and 7.4 fitted well with the first-order kinetic ($R^2 = 0.989$) and Korsmeyer–Peppas model ($R^2 = 0.991$), respectively. Meanwhile, the percent

cumulative release (within 24 h) in PBS at pH 5.8 and 7.4 was found to be 41.56% and 68.46%, respectively. At low concentrations, Fe-MIL100 is found to be non-toxic to normal cells.

Acknowledgements

Financial support from the Ministry of Research and Technology and Higher Education through a Fundamental Research project with the contract no 130S/WM01.5/N/2020 is highly appreciated.

Author contributions

YD and IA contributed to data acquisition and interpretation; YD, IA, MY, and SBH were involved in analysis and data interpretation; SI and FES contributed to conceptualization; YD, IA, AEA, and PLT-N were involved writing—original draft; FES, WI, and SI contributed to funding acquisition; and SI, SPS and YHJ were involved in writing—review and editing.

Compliance with ethical standards

Conflict of interest The authors declare no conflict of interest.

Electronic supplementary material: The online version of this article (<https://doi.org/10.1007/s10853-020-05009-3>) contains supplementary material, which is available to authorized users.

References

- Zhang W, Wang Y, Zheng H, Li R, Tang Y, Li B, Zhu C, You L, Gao M-R, Liu Z, Yu S-H, Zhou K (2020) Embedding ultrafine metal oxide nanoparticles in monolayered metal-organic framework nanosheets enables efficient electrocatalytic oxygen evolution. *ACS Nano* 14:1971–1981
- Li R, Yuan S, Zhang W, Zheng H, Zhu W, Li B, Zhou M, Law AW-K, Zhou K (2019) 3D printing of mixed matrix films based on metal-organic frameworks and thermoplastic polyamide 12 by selective laser sintering for water applications. *ACS Appl Mater Interfaces* 11:40564–40574
- Li R, Zhang W, Zhou K (2018) Metal-organic-framework-based catalysts for photoreduction of CO₂. *Adv Mater* 30:1705512
- Zhang W, Kauer M, Halbherr O, Epp K, Guo P, Gonzalez MI, Xiao DJ, Wiktor C, Xamena FXLi, Wöll C, Wang Y, Muhler M, Fischer RA (2016) Ruthenium metal-organic frameworks with different defect types: influence on porosity, sorption, and catalytic properties. *Chem A Eur J* 22:14297–14307
- Gupta V, Tyagi S, Paul AK (2019) Development of biocompatible iron-carboxylate metal organic frameworks for pH-responsive drug delivery application. *J Nanosci Nanotechnol* 16:646–654
- Siafka PI, Üstündağ ON, Karavas E, Bikiaris DN (2016) Surface modified multifunctional and stimuli responsive nanoparticles for drug targeting: current status and uses. *Int J Mol Sci* 17:E1440
- Huxford RC, Rocca JD, Lin W (2010) Metal-organic frameworks as potential drug carriers. *Curr Opin Chem Biol* 14:262–268
- Guesh K, Caiuby CAD, Mayoral A, Diaz-Garcia M, Diaz I, Shancez-Sanchez M (2017) Sustainable preparation of MIL-100(Fe) and its photocatalytic behavior in the degradation of methyl orange in water. *Cryst Growth Des* 17:1806–1813
- Sun C-Y, Qin C, Wang X-L, Su Z-M (2012) Metal-organic frameworks as potential drug delivery systems. *Expert Opin Drug Deliv* 10:89–101
- Mizutani M, Maejima N, Jitsukawa K, Masuda H, Einaga H (1998) An infinite chiral single-helical structure formed in Cu(II)-L-/D-glutamic acid system. *Inorg Chim Acta* 283:105–110
- Torre BGdl, Albericio F (2019) The pharmaceutical industry in 2018. An analysis of FDA drug approvals from the perspective of molecules. *Molecules* 24:809–820
- Taherzade S, Soleimannejad J, Tarlani A (2017) Application of metal-organic framework nano-MIL-100(Fe) for sustainable release of doxycycline and tetracycline. *Nanomaterials* 7:215
- Rocca JD, Liu D, Lin W (2011) Nanoscale metal-organic frameworks for biomedical imaging and drug delivery. *Acc Chem Res* 44:957–968
- Haydar MA, Abid HR, Sunderland B, Wang S (2019) Multimetal organic frameworks as drug carriers: aceclofenac as a drug candidate. *Drug Des Devel Ther* 13:23–35
- Simon MA, Anggraeni E, Soetaredjo FE, Santoso SP, Irawaty W, Thanh TC, Hartono SB, Yuliana M, Ismadji S (2019) Hydrothermal synthesise of HF free MIL-100(Fe) for isoniazid-drug delivery. *Sci Rep* 9:16907
- Rojas S, Colinet I, Cunha D, Hidalgo T, Salles F, Serre C, Guillou N, Horcajada P (2018) Toward understanding drug incorporation and delivery from biocompatible metal-organic frameworks in view of cutaneous administration. *ACS Omega* 3:2994–3003

- [17] Zhu Y-D, Chen S-P, Zhao H, Yang Y, Chen X-Q, Sun J, Fan H-S, Zhang X-D (2016) PPy@MIL-100 nanoparticles as a pH- and near-IR-irradiation-responsive drug carrier for simultaneous photothermal therapy and chemotherapy of cancer cells. *ACS Appl Mater Interfaces* 8:34209–34217
- [18] Granero GE, Longhi MR, Becker C, Junginger HE, Kopp S, Midha KK, Shah VP, Stavchansky S, Dressman JB, Barends DM (2008) Biowaiver monographs for immediate release solid oral dosage forms: acetazolamide. *J Pharm Sci* 97:3691–3699
- [19] Ai H, Jones SA, Villiers MMD, Lvov YM (2003) Nanocapsulation of furosemide microcrystals for controlled drug release. *J Control Release* 86:59–68
- [20] Brewster ME, Loftsson T (2007) Cyclodextrins as pharmaceutical solubilizers. *Adv Drug Deliv Rev* 10:231–242
- [21] Dehghan MH, Jafar M (2010) Improving dissolution of meloxicam using solid dispersions. *Iran J Pharm Re* 4:231–238
- [22] Doherty C, York P (1989) Microenvironmental pH control of drug dissolution. *Int J Pharm* 50:223–232
- [23] Latif R, Halim SAA, Kader OMA (2013) Furosemide loaded superporous hydrogel composite as a controlled release device: different strategies for drug loading. *J Pharm Res Opin* 6:28–35
- [24] Patel RC, Keraliya RA, Patel MM, Patel NM (2010) Formulation of Furosemide solid dispersion with micro crystalline cellulose for achieve rapid dissolution. *J Adv Pharm Technol Res* 1:180–189
- [25] Shihab FA, Ebian AR, Mustafa RM (1979) Effect of polyethylene glycol, sodium lauryl sulfate and polysorbate-80 on the solubility of Furosemide. *Int J Pharm* 4:13–20
- [26] Shukla A, Singh AP, Ray B, Aswal V, Kar AG, Maiti P (2018) Efficacy of polyurethane graft on cyclodextrin to control drug release for tumor treatment. *J Colloid Interface Sci* 534:215–227
- [27] Singh G, Pai RS, Devi VK (2011) Effects of the eudragit and drug coat on the release behavior of poorly soluble drug by solid dispersion technique. *Int J Pharm Sci Res* 2:816–824
- [28] Putz H, Brandenburg K Match!—phase identification from powder diffraction, crystal impact, Kreuzherrenstr. 102, 53227 Bonn, Germany, <https://www.crystalimpact.de/match>.
- [29] Putro JN, Ismadji S, Gunarto C, Yuliana M, Santoso SP, Soetaredjo FE, Ju YH (2019) The effect of surfactants modification on nanocrystalline cellulose for paclitaxel loading and release study. *J Mol Liq* 282:407–414
- [30] Marshall CR, Staudhammer SA, Brozek CK (2019) Size control over metal-organic framework porous nanocrystals. *Chem Sci* 10:9396–9408
- [31] Angkawijaya AE, Santoso SP, Soetaredjo FE, Ismadji S, Ju YH (2015) Equilibrium study of complex formation among trivalent metals, glycine peptides and phenolates in aqueous solution. *J Solution Chem* 44:2129–2143
- [32] Santoso SP, Ismadji S, Angkawijaya AE, Soetaredjo FE, Go AW, Ju YH (2016) Complexes of 2,6-dihydroxybenzoic acid with divalent metal ions: synthesis, crystal structure, spectral studies, and biological activity enhancement. *J Mol Liq* 221:617–623
- [33] Shan B, James JB, Armstrong MR, Close EC, Letham PA, Nikkiah K, Lin YS, Mu B (2018) Influences of deprotonation and modulation on nucleation and growth of UiO-66: intergrowth and orientation. *J Phys Chem C* 122:2200–2206
- [34] Sánchez-Sánchez M, Getachew N, Díaz K, Díaz-García M, Chebude Y, Díaz I (2015) Synthesis of metal-organic frameworks in water at room temperature: salts as linker sources. *Green Chem* 17:1500–1509
- [35] Horcajada P, Surlé S, Serre C, Hong DY, Seo YK, Chang JS, Grenèche JM, Margiolaki I, Férey G (2007) Synthesis and catalytic properties of MIL-100(Fe), an iron(III) carboxylate with large pores. *Chem Commun* 27:2820–2822
- [36] Huang S, Yang KL, Liu XF, Pan H, Zhang H, Yang S (2017) MIL-100(Fe)-catalyzed efficient conversion of hexoses to lactic acid. *RSC Adv* 7:5621–5627
- [37] Tan F, Liu M, Li K, Wang Y, Wang J, Guo X, Zhang G, Song C (2015) Facile synthesis of size-controlled MIL-100(Fe) with excellent adsorption capacity for methylene blue. *Chem Eng J* 281:360–367
- [38] Campagnol N, Assche TV, Boudewijns T, Denayer J, Binne-mans K, Vos DD, Fransaeer J (2013) High pressure, high temperature electrochemical synthesis of metal-organic frameworks: films of MIL-100 (Fe) and HKUST-1 in different morphologies. *Mater Chem A* 1:5827–5830
- [39] Al-Haydar M, Abid HR, Sunderland B, Wang S (2017) Metal organic frameworks as a drug delivery system for flurbiprofen. *Drug Des Devel Ther* 11:2685–2695
- [40] Nethaji S, Sivasamy A, Mandal AB (2013) Adsorption isotherms, kinetics and mechanism for the adsorption of cationic and anionic dyes onto carbonaceous particles prepared from *Juglans regia* shell biomass. *Int J Environ Sci Technol* 10:231–242
- [41] Hasan Z, Jeon J, Jung SH (2012) Adsorptive removal of naproxen and clofibrac acid from water using metal-organic frameworks. *J Hazard Mater* 209–210:151–157
- [42] Al-Muhtaseb AH, Ibrahim KA, Albadarin AB, Ali-khashman O, Walker GM, Ahmad MNM (2011) Remediation of phenol-contaminated water by adsorption using poly(methyl methacrylate) (PMMA). *Chem Eng J* 168:691–699
- [43] Irving L (1918) The adsorption of gases on plane surfaces of glass, mica and platinum. *J Am Chem Soc* 40:1361–1403
- [44] Mota FL, Carneiro AP, Queimada AJ, Pinho SP, Macedo EA (2009) Temperature and solvent effects in the solubility

- of some pharmaceutical compounds: measurements and modeling. *Eur J Pharm Sci* 37:499–507
- [45] London BK, Claville MOF, Babu S, Fronczek FR, Uppu RM (2015) A co-crystal of nonahydrated disodium(II) with mixed anions from m-chlorobenzoic acid and Furosemide. *Acta Crystallogr Sect E Crystallogr Commun* 71:1266–1269
- [46] Bellido E, Guillevic M, Hidalgo T, Santander-Ortega MJ, Serre C, Horcajada P (2014) Understanding the colloidal stability of the mesoporous MIL-100(Fe) nanoparticles in physiological media. *Langmuir* 30:5911–5920
- [47] Verhoeven J, Peschier LJC, Danhof M, Junginger HE (1988) A controlled-release matrix tablet of Furosemide: design, in vitro evaluation, pharmacological and pharmacodynamic evaluation. *Int J Pharm* 45:65–77
- [48] Lin CX, Qiao SZ, Yu CZ, Ismadji S, Lu GQ (2009) Periodic mesoporous silica and organosilica with controlled morphologies as carriers for drug release. *Micropor Mesopor Mater* 117:213–219
- [49] Kormsmeier RW, Gurny R, Doelker E, Buri P, Peppas NA (1983) Mechanisms of solute release from porous hydrophilic polymers. *Int J Pharm* 15:25–35
- [50] Nabipour H, Sadr MH, Bardajee GR (2017) Release behavior, kinetic and antimicrobial study of nalidixic acid from [Zn2(bdc)2(dabco)] metal-organic frameworks. *J Coord Chem* 70:2771–2784
- [51] Jain A, Thakur K, Kush P, Jain UK (2014) Docetaxel loaded chitosan nanoparticles: formulation, characterization and cytotoxicity studies. *Int J Biol Macromol* 69:546–553
- [52] Horcajada P, Chalati T, Serre C, Gillet B, Sebrie C, Baati T, Eubank JF, Heurtaux D, Clayette P, Kreuz C, Chang JS, Hwang YK, Marsaud V, Bories PN, Cynober L, Gil S, Férey G, Couvreur P, Gref R (2010) Porous metal-organic-framework nanoscale carriers as a potential platform for drug delivery and imaging. *Nat Mater* 9:172–178

Publisher's Note Springer Nature remains neutral with regard to jurisdictional claims in published maps and institutional affiliations.